RESEARCH PAPER

Improved cytotoxicity of paclitaxel loaded in nanosized lipid carriers by intracellular delivery

Jing Miao · Yongzhong Du · Hong Yuan ·
Xingguo Zhang · Qian Li · Yuefeng Rao ·
Mengdan Zhao · Fuqiang Hu

Abstract Nanosized lipid carriers (NLC) can improve the limited drug-loading (DL) capacity and drug expulsion during storage, and adjust the drug release profile of solid lipid nanoparticles (SLN). In this study, Paclitaxel (PTX)-loaded NLC were prepared by solvent diffusion method using monostearin as solid lipid and oleic acid (OA) as liquid lipid matrix. The blank NLC with different OA content (the size range was from 89.5 ± 7.4 to 160.2 ± 34.6 nm) showed smaller size than the blank SLN (the size was 272.7 ± 43.6 nm), while the PTX-loaded NLC (the size range was from 481.3 ± 29.8 to 561.7 ± 38.3 nm) showed little bigger size, higher DL capacity, and faster drug in vitro release rate comparing with SLN (the size was 437.3 ± 68.2 nm). The 50 % cellular growth inhibitions (IC_{50}) of PTX-loaded NLC with 0, 5, 10, and 20 wt % OA were 0.92 ± 0.06, 0.69 ± 0.04, 0.25 ± 0.02, and 0.12 ± 0.02 $\mu g \ mL^{-1}$, respectively, while the IC_{50} of Taxol^{TM} was 1.72 ± 0.09 $\mu g \ mL^{-1}$. For analyzing cellular drug effect, cellular uptakes of fluorescent NLC and intracellular drug concentration were investigated. As the incorporation of OA into solid lipid matrix could accelerate both the cellular uptake and the PTX delivery, loaded by NLC, the cytotoxicity of PTX could be enhanced, and further enhanced by increasing OA content in NLC.

Keywords Nanosized lipid carriers · Paclitaxel · Cytotoxicity · Cellular uptake · Intracellular delivery · Nanomedicine

J. Miao (✉) · X. Zhang · Q. Li · Y. Rao
Department of Pharmacy, the First Affiliated Hospital, College of Medicine, Zhejiang University, 79 Qingchun Road, Hangzhou 310003, People's Republic of China
e-mail: joemj1005@163.com; miaojing@zju.edu.cn

Y. Du · H. Yuan · F. Hu (✉)
College of Pharmaceutical Sciences, Zhejiang University, 866 Yuhangtang Road, Hangzhou 310058, People's Republic of China
e-mail: hufq@zju.edu.cn

M. Zhao
Women's Hospital, College of Medicine, Zhejiang University, 2 Xueshi Road, Hangzhou 310006, People's Republic of China

Introduction

One of the major difficulties in cancer therapy is targeting anticancer drugs to their sites of action in the body. After administration, most anticancer drugs distribute without selectivity, thus cause many problems such as toxicity toward healthy tissues. Drug targeting can improve the efficacy of therapy and reduce side effects associated with anticancer drugs. Up to now, some colloidal drug carriers such as liposomes (Drummond et al. 1999), nanoparticles (Brigger et al. 2002), polymeric micelles (Garrec et al. 2004), and nanorattles (Hu et al. 2011) have been used

to encapsulate some anticancer drugs for altering their pharmacokinetic and biodistribution profiles. These nanoscopic systems can enhance drug accumulation at the tumor site and reduce distribution to healthy tissues. However, the ideal molecular target site for anticancer drug has not been established. Site-specific delivery of drug receives a lot of attention because it can further reduce drug toxicity and increase therapeutic effects. Therefore, we need to find a kind of carrier with low toxicity, good biocompatibility, and high efficient intracellular delivery.

Nanosized lipid carriers (NLC), a new generation of solid lipid nanoparticles (SLN), have been looked upon as a promising carrier with several attractive features for drug delivery. NLC can overcome the limitations associated with the SLN, namely, limited DL, risk of gelation, and drug leakage during storage caused by lipid polymorphism (Müller et al. 2002a). NLC are prepared by mixing solid lipids with liquid lipids. The resulting matrix of lipid particles shows great imperfections in the crystal lattice and leaves enough space to accommodate drug molecules, thus, leading to improved drug loading (DL) capacity (Jenning et al. 2000a; Jenning et al. Jenning and Gohla 2001; Souto et al. 2004a). Besides, NLC remain its solid state by controlling the liquid lipid content added to the formulation, and therefore, the controlled drug release properties can be achieved (Müller et al. 2002b).

Paclitaxel (PTX) is an effective chemotherapeutic agent against a wide spectrum of solid tumors. However, the poor aqueous solubility has limited the clinical formulations of PTX. The sole commercial product is Taxol[TM], which consists of PTX solubilized at 6 mg mL^{-1} (7 mM) in a 1:1 mixed solvent of Cremophor EL[®] (CrEL, polyoxyethylated castor oil) and ethanol. It has been reported that Cremophor EL may cause serious adverse effects including acute hypersensitivity reactions and neurological toxicity (Gelderblom et al. 2001). In our previous study, SLN could transport PTX to the target cells selectively and efficiently, and improve the in vitro drug effect (Yuan et al. 2008; Miao et al. 2013). Therefore, it is promising to increase DL capacity of PTX, and transport PTX to the target cells more efficiently via NLC.

Up to now, the special features of NLC, such as the improved drug entrapment efficiency (EE) and controlled drug release properties (Jenning et al. 2000a;

Souto et al. 2004a; Hu et al. 2005; Yuan et al. 2008), the morphological characterization (Jores et al. 2004; Souto et al. 2004b), the possibility of topical usage, the crystal order by differential scanning calorimetry (DSC) (Castelli et al. 2005) and ^{1}HNMR (Jenning et al. 2000b), and the reversal activity loading cytotoxic drug in multi-drug-resistant cancer cells (Zhang et al. 2008) has been studied by many different groups including ours. However, few detail works were conducted to analyze the therapeutic effect of drug-loaded NLC with different liquid lipids content.

In this study, PTX was chosen as the model drug, A549 cells were chosen as the model cells, and the cytotoxicities of PTX-loaded monostearin (MS) NLC with different oleic acid (OA) contents were investigated. Focussing on the mechanism of enhanced cytotoxicity of PTX delivered by NLC, we also analyze the cellular uptakes of fluorescent NLC, the in vitro release profiles, and the cellular uptakes of PTX loaded in NLC.

Materials and methods

Materials

MS was purchased from Shanghai Chemical Reagent Co. Ltd., China. OA, 1-Ethyl-3-(3-dimethylaminopropyl) carbodiimide (EDC), and 3-(4,5-dimethylthiazol-2-yl)-2,5-diphenyl-tetrazolium bromide (MTT) were purchased from Sigma, USA. Octadecylamine (ODA) was purchased from Fluka, USA. Fluorescein isothiocyanate (FITC) was purchased from Acros Organic, USA. The surfactant, poloxamer 188, was provided by Shenyang Pharmaceutical University Jiqi Co. Ltd., China. PTX was purchased from Zhanwang Biochemical Co. Ltd., China. Fetal bovine serum (FBS) was provided by Zhejiang Sijiqing Biotechnology Co. Ltd., China. Trypsin and RPMI Medium 1640 were purchased from Amresco Inc., solon, OH, USA and Gibco BRL, Gaithersburg, MD, USA, respectively.

Cell lines

A549 cells, human cell line derived from the respiratory epithelium cells, were obtained from Cell Resource Center of China Science Academe. The cells were cultured at 37 °C with 5 % CO$_2$ and under fully humidified conditions. The culture medium was

RPMI1640 supplemented with 10 % FBS, 100 units mL^{-1} penicillin, and 100 units mL^{-1} streptomycin.

Synthesis of FITC–ODA

The method for synthesis of FITC–ODA was reported in our previous research (Yuan et al. 2008). Briefly, 7 mg ODA was completely dissolved in 60 mL N, N-dimethylformamide (DMF) by sonicate treatment (Sonic Purger CQ250, Academy of Shanghai Shipping Electric Instrument). 20 mg FITC was dissolved in 5 mL DMF. The FITC and ODA solutions were then mixed and shaked (HZ-8812S, Hualida Co. Ltd) in water bath at 50 °C for 48 h. After reaction, the reaction mixture was cooled to room temperature, and 20 mL of distilled water was then added to the mixture to precipitate the FITC–ODA. The precipitate was collected by filtration with 0.45-µm Millipore filter and washed twice by 20 mL distilled water. The final product (FITC–ODA) was lyophilized and stored in dark for further use.

Preparation of nanoparticles

Figure 1 demonstrates the process of preparation of NLC. The NLC with or without PTX were prepared by solvent diffusion method in an aqueous system reported in our previous study (Zhang et al. 2008). Briefly, 60 mg lipid materials (MS with 0–20 wt % OA) with or without 3 mg PTX were completely dissolved into 6 mL ethanol in water bath of 70 °C. Then the organic solution was dispersed into 60 mL distilled water as quickly as possible, under 400 rpm mechanical agitate for 5 min still in water bath of 70 °C. The obtained pre-emulsion was cooled to room temperature, which was the NLC dispersion.

For preparing the fluorescent NLC, 9 mg FITC–ODA was added to 51 mg lipid materials (MS with 0-20 wt % OA).

The NLC dispersion was adjusted to pH 1.20 by adding 0.1 M hydrochloric acid to form the precipitate of NLC and collected by centrifugation (46,282×g for 15 min, 3K30, Sigma, Germany) for drug entrapment efficiency and DL determination.

The NLC precipitate was re-dispersed in the aqueous solution containing 0.1 % poloxamer 188 (w/v) by probe-type ultrasonic treatment with 20 sonic bursts (200 W, active every 2 s for a 3 s duration) (JY92-II, Scientz Biotechnology Co., Ltd., China). Then the resultant dispersion was fast frozen under −64 °C in a deep-freezer (Sanyo Ultra-Low-Temperature Freezer MDF-192, Japan) for 5 h, and then the sample was moved to the freeze-drier (Freezone 2.5L, LABCONCO, USA). The drying time was controlled in 72 h, and then the NLC powders were collected for in vitro release study, cellular drug effect, and intracellular drug concentration determination.

Particle size and zeta potential measurement

The volume average diameter and zeta potential of blank or drug-loaded NLC in dispersion were determined by Zetasizer (3000HS, Malvern Instruments, UK) after diluted 20 times with distilled water.
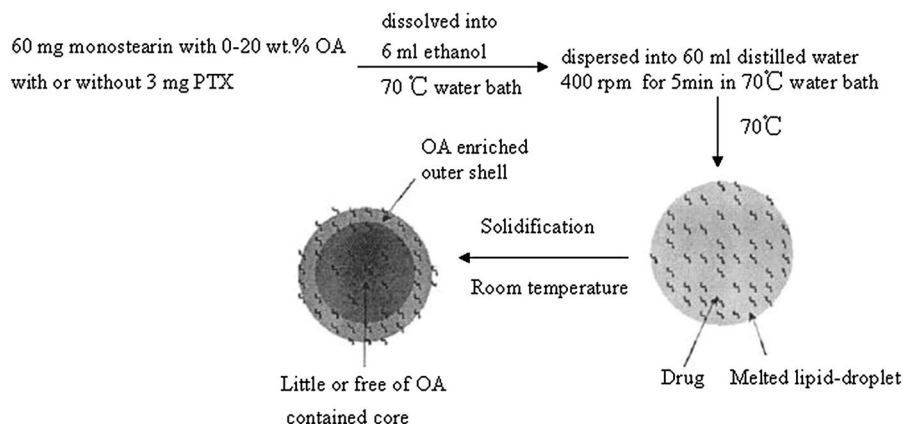
Fig. 1 Schematic of preparation process of NLC

Determination of drug entrapment efficiency and DL

As the precipitate of NLC was received by the centrifugation, the drug content in the supernatant was separated and measured by HPLC method (Agilent 1100 series, USA). The mobile phase was a mixture of acetonitrile and water (50:50 v/v). The column was Diamohsil^{TM} C18 (250 × 4.6 mm) with 5 μm particles. The flow rate was 1.0 mL min^{-1}, the detection wavelength was 227 nm (G1314A, JP11615541, UV detector, USA), and the column temperature was maintained at 35 °C. Injected volume of the sample was 20 μL (Hu et al. 2006). The calibration curve of peak area against concentration of PTX was y = 32.361x −16.282 under the concentration of PTX 0.5–120 μg mL^{-1} (R^2 = 0.9994, where y = peak area and x = PTX concentration), and the detection limit was 0.01 μg mL^{-1}.

The separated NLC were re-dispersed in 100 mL of PBS solution (containing 2 M sodium salicylate, pH 7.4) and surged by vortexing (XW-80A, Instruments factory of Shanghai Medical University, China) for 3 min to dissolve the drugs on the surface of NLC. The dispersions were then centrifuged (3K30, Sigma, Germany) for 15 min at 46,282×g. The drug content in the supernatant after centrifugation was measured by HPLC method as described above. The drug EE and DL of NLC were calculated from Eqs. (1) and (2).

$$EE = (Wa − Ws_1 − Ws_2)/Wa \times 100\%. \qquad (1)$$

$$DL = (Wa − Ws_1 − Ws_2)/(Wa − Ws_1 − Ws_2 + W_L) \times 100\%, \qquad (2)$$

where Wa was the weight of drug added in system, Ws_1 was the analyzed weight of drug in supernatant after the first centrifugation, Ws_2 was the analyzed weight of drug in supernatant after the second centrifugation, and W_L was the weight of lipid added in system.

TEM examination

The morphological observation of drug-loaded nanoparticles was performed by transmission electron microscopy (TEM) (TECNAI 10, PHILIPS, Dutch). The samples were diluted for TEM observation.

Atomic force microscopy (AFM) investigation

The surface properties of drug-loaded nanoparticles were visualized by an AFM (SPA 3800 N, SEIKO, Japan). Explorer atomic force microscope was in tapping mode, using high resonant frequency (F_0 = 129 kHz) pyramidal cantilevers with silicon probes having force constants of 20 N m^{-1}. Scan speeds were set at 2 Hz.

The samples were diluted 10 times with distilled water and then dropped onto freshly cleaved mica plates, followed by vacuum drying during 24 h at 25 °C.

In vitro drug release study

The drug release profiles from nanoparticles were measured in vitro. 30 mg of powdered SLN or NLC were re-dispersed in 100 mL of PBS (pH 7.4) containing 2 M sodium salicylate and mixed by vortexing at 2,800 rpm for 3 min, and then shaken horizontally (Shellab 1227-2E, Shellab, USA) at 37 °C and 60 strokes min^{-1} for 24 h. One milliliter of the dispersion was withdrawn from the system at definite time interval and filtrated with 0.22-μm filter. The filtrate was determined by HPLC method as described above.

Cellular drug effect

A549 were seeded in a 96-well plate at a seeding density of 10,000 cells per well in 0.2 mL of growth medium consisting of RPMI1640 with 10 % FBS and antibiotics. A549 were cultured at 37 °C for 24 h. The growth medium was then removed, and growth medium containing different concentrations of Taxol (PTX solved in 50:50 mixture of Cremophor EL and ethanol) and different lipid concentrations of NLC without drug or loading PTX was added, respectively. The cells were further incubated for 48 h. After incubation, the metabolic activities of the cells were measured. Each well was added with 100 μL fresh growth medium containing 50 mg MTT and then incubated for 4 h. The unreduced MTT and medium were removed in each well, followed by washing with 100 μL of PBS, and then 180 μL DMSO was added to dissolve formazan crystals of MTT. The absorbance of formazan was measured at 570 nm in a microplate

reader (BioRad, Model 680, USA). Survival percentage was calculated as compared to mock-treated cells (100 % survival). All the experiments were performed in triplicate.

Cellular uptakes of fluorescent nanoparticles

A549 were seeded in a 24-well plate at a seeding density of 10,000 cells per well in 1 mL of growth medium and allowed to attach for 24 h. A549 were incubated with FITC–ODA-loaded NLC suspension (the concentration were 100 μg mL^{-1}) in growth medium for different time. After the incubation, cells were washed thrice with PBS (pH 7.4) to remove the fluorescent NLC adsorbed on the cell membrane, and then directly viewed under a fluorescence microscope (Leica DM4000 B, Leica, Germany).

To assay the cellular uptakes quantitatively, after the cells washed with PBS, 40 μL trypsin PBS solution (2.5 mg mL^{-1}) was added. The cells were further incubated for 5 min. Then the cells were harvested by adding 1 mL PBS. The harvested cells were treated by probe-type ultrasonication for 5 times (4 °C, 200 W, active every 5 s for a 60 s duration) to be broken. The cell lysate was centrifuged (22,360$\times g$ for 10 min), and the fluorescence intensity of supernatant was measured using fluorometer (F-4000, HITACHI Co., Japan) (excitation: 490 nm; emission: 528 nm). The uptake percentages of NLC were calculated from Eqs. (3).

$$\text{Uptake percentage } (\%) = F/F_0 \times 100\%, \qquad (3)$$

where F was fluorescence intensity in different times, and F_0 was initial fluorescence intensity of the fluorescent NLC.

Intracellular drug concentration determination

10^4 A549 were plated in 24-well plates and grown for 24 h, and then incubated with Taxol (2 μg mL^{-1}), PTX-loaded NLC with 0–20 wt % OA content (drug concentration: 2 μg mL^{-1}) in growth medium for 1, 2, 4, 12, and 24 h. After the cells were washed thrice with PBS, 100 μL trypsin PBS solution (2.5 mg mL^{-1}) was added. The cells were further incubated for 5 min. According to the method reported by our previous literature (Yuan et al. 2008), by adding 400 μL methanol, and following centrifugation (22,360$\times g$

for 10 min), the cell lysate was harvested. The drug content in the supernatant was measured by HPLC method, while the protein content in the cell lysate was measured using Micro BCA protein assay kit. The drug uptake percentage was calculated from Eqs. (4).

$$\text{Drug uptake percentage } (\%)$$
$$= (C/M) / (C_0/M_0) \times 100\%, \qquad (4)$$

where C was intracellular concentration of PTX in different time, M was the weight (milligram) of cellular protein in different time, C_0 was initial concentration of PTX, and M_0 was initial weight (milligram) of cellular protein.

Results

Preparation and characterization of NLC

The volume average diameter, polydispersity indexes, and zeta potential of fluorescent NLC and PTX-loaded NLC with different OA contents are listed in Table 1. Due to the NLC used in the cellular uptake and cytotoxicity tests were the NLC redispersions in 0.1 % poloxamer 188 solutions, the results were the data of NLC redispersions. In Table 1, NLC without PTX show a size decrease with OA content increase. However, PTX-loaded NLC with 0, 5, and 10 wt % OA showed a size increase, while PTX-loaded NLC with 20 wt % OA showed a particle size decrease against PTX-loaded NLC with 10 wt % OA. In addition, the sizes of PTX-loaded NLC were bigger than that of fluorescent ones.

Zeta potential is a key factor to evaluate the stability of colloidal dispersion. In general, particles could disperse stably when the absolute value of zeta potential was above 30 mV due to the electric repulsion between particles (Müller et al. 2001). As shown in Table 1, all of the absolute values of zeta potential for obtained NLC were above 30 mV; this demonstrated that the nanoparticles redispersion was a physically stable system.

The results of EE and DL of PTX-loaded NLC are also given in Table 1. As OA content increased, the EE of PTX was improved from 61.83 ± 1.70 to 77.63 ± 0.47 %, and the DL of PTX was improved from 2.92 ± 0.15 to 3.74 ± 0.02 %.

Table 1 Properties of resulted fluorescent NLC and PTX-loaded NLC. ($n = 3$)

OA content (%)	Fluorescent NLC			PTX-loaded NLC				
	d_v (nm)	PI (−)	ζ (−mV)	d_v (nm)	PI (−)	ζ (−mV)	EE (%)	DL (%)
0	272.7 ± 43.6	0.101 ± 0.015	36.4 ± 2.1	437.3 ± 68.2	0.436 ± 0.068	41.2 ± 5.2	61.83 ± 1.70	2.92 ± 0.15
5	160.2 ± 34.6	0.314 ± 0.034	40.2 ± 2.9	481.3 ± 29.8	0.300 ± 0.028	46.6 ± 2.1	64.40 ± 3.61	3.21 ± 0.11
10	134.4 ± 21.0	0.361 ± 0.024	45.5 ± 3.0	561.7 ± 38.3	0.382 ± 0.039	37.4 ± 2.8	68.67 ± 4.50	3.42 ± 0.17
20	89.5 ± 7.4	0.337 ± 0.016	49.0 ± 2.7	531.4 ± 23.1	0.189 ± 0.021	36.5 ± 3.2	77.63 ± 0.47	3.74 ± 0.02

d_v, PI, ζ, EE, and DL indicate the volume average diameter, polydispersity index, zeta potential, drug entrapment efficiency, and drug loading, respectively

TEM examination

Figure 2 shows the transmission electron micrographs of drug-loaded NLC with 0 and 10 wt % OA content. The TEM photographs revealed that NLC with 10 wt % OA content appeared in the formation of spherical nanoparticles with larger particle size. On the contrary, NLC without OA content (0 wt %) appeared in quasi-sphere and cylinder-like irregular shapes, and with smaller particle size.

AFM investigation

To investigate the difference of three-dimensional structure between SLN and NLC, we analyzed the tapping mode AFM images of PTX-loaded NLC with 0 and 10 wt % OA content. In Fig. 3a, the images of NLC without OA (SLN) show severely flattened objects of about 400 nm in diameter, but only about 10 nm in height. In Fig. 3b, the NLC with 10 wt % OA were somewhat flattened objects of about 500 nm in diameter, and about 100 nm in height. The observed flattened particles in AFM image may result from the collapse of nanoparticles during vacuum drying process (Montasser et al. 2002). From Fig. 3, it was also found that the shape of NLC was more spherical than that of SLN, which may explain why the NLC was less severely flattened.

In vitro release profiles

The drug release profiles from PTX-loaded NLC prepared by the solvent diffusion method at 70 °C are shown in Fig. 4. The release rate became faster when
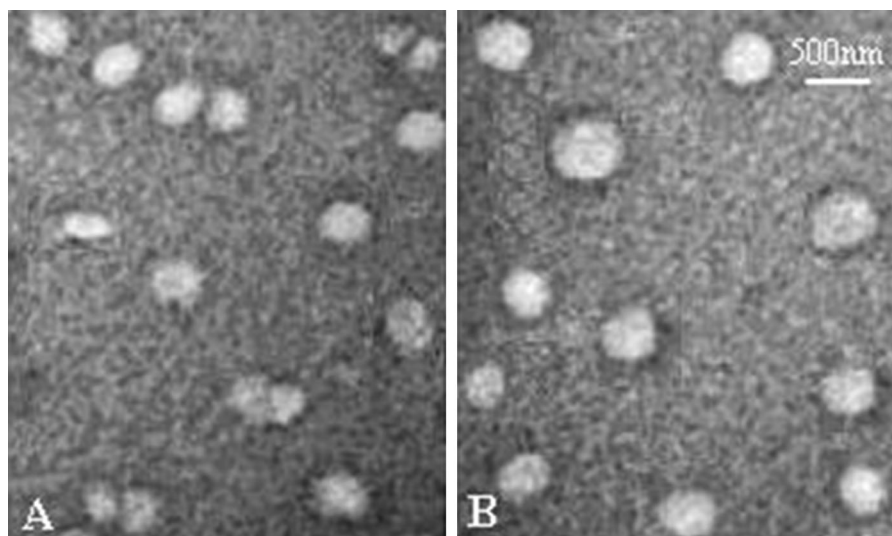
Fig. 2 Transmission electron microscopy micrographs of PTX-loaded NLC. The bars are 500 nm. **a** NLC without OA; **b** NLC with 10 wt % OA

Fig. 3 Atomic force microscopy images of PTX-loaded NLC. **a** NLC without OA; **b** NLC with 10 wt % OA
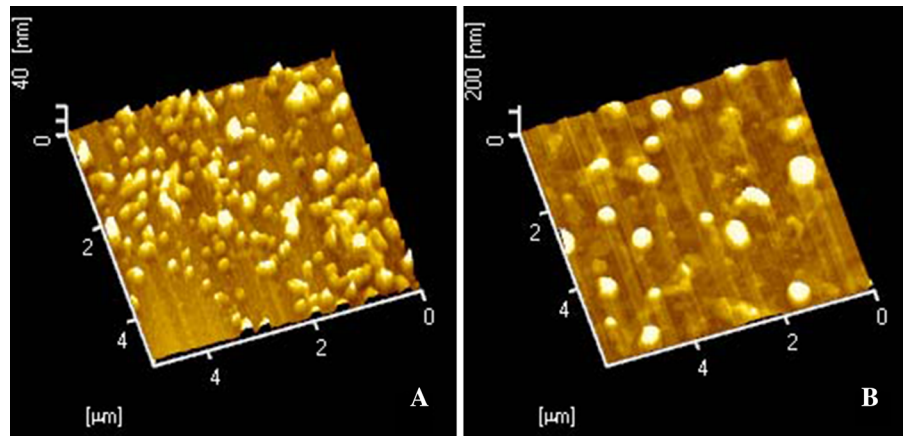
OA was incorporated into nanoparticles and further accelerated with the increase of OA content.
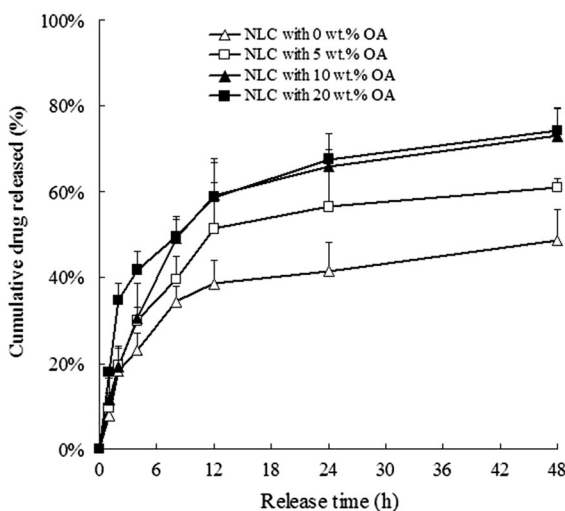
Cellular drug effect

The cytotoxicities of blank NLC are shown in Table 2. As a kind of biocompatible solid lipid material, the IC$_{50}$ value of MS was $396.82 \pm 33.19 \ \mu g \ mL^{-1}$, which indicated a low cytotoxicity. After adding FITC–ODA or different OA contents, the IC$_{50}$ values of NLC were still above about $300 \ \mu g \ mL^{-1}$, indicating that these materials were safe for modifying NLC.

Table 2 also reports the IC$_{50}$ value of Taxol and PTX-loaded NLC against A549 cells. Comparing with

Table 2 Cytotoxicities of blank NLC, Taxol, and PTX-loaded NLC

Formulation	IC$_{50}$ ($\mu g \ mL^{-1}$)
Blank NLC	
Monostearin only	396.82 ± 33.19
Monostearin + 15 wt % FITC–ODA	362.88 ± 37.24
Monostearin + 5 wt % OA	303.56 ± 33.17
Monostearin + 10 wt % OA	298.40 ± 30.95
Monostearin + 20 wt % OA	290.51 ± 31.82
Taxol	1.72 ± 0.09
PTX-loaded NLC	
PTX-loaded NLC with 0 wt % OA	0.92 ± 0.06
PTX-loaded NLC with 5 wt % OA	0.69 ± 0.04
PTX-loaded NLC with 10 wt % OA	0.25 ± 0.02
PTX-loaded NLC with 20 wt % OA	0.12 ± 0.02

the Taxol, the cytotoxicity of PTX could be enhanced after encapsulated by NLC, and further enhanced as OA content increased. Calculating data from Table 2, the cytotoxicities of NLC with 0, 5, 10, and 20 wt % OA content were 1.9-, 2.5-, 6.9-, and 14.3-fold higher than that of Taxol, respectively.

Cellular uptakes of fluorescent NLC

As reported previously (Yuan et al. 2008), the fluorescent lipid nanoparticles indicated above 97 % FITC–ODA incorporation efficiency, and the leakage of FITC–ODA from lipid nanoparticles was lower than 7 % in vivo transport. Due to this reason, the fluorescent NLC marked by FITC–ODA were used to evaluate the cellular uptakes of NLC. Choosing A549

Fig. 4 In vitro PTX release profiles of PTX-loaded NLC with different OA contents

cancer cells as the model cells, the cellular uptakes of NLC with different OA contents were observed by fluorescence microscopy. To remove fluorescent NLC adsorbed on the cell membrane, the cells were washed thrice with PBS. Moreover, after incubating with FITC solution for 24 h, no fluorescence was found inside A549 cells. It indicated that FITC molecule could not be uptaken by A549 cells.

Figure 5 shows the fluorescence images when the cells were incubated with NLC with different OA contents for different incubation times at the same incubation concentration of NLC (100 μg mL^{-1}). It can be seen that the fluorescence intensity inside A549 cells increased with incubation time in all runs. It means the cellular uptake of NLC was time-dependent. As shown in Fig. 5, there was no significant fluorescence inside A549 cells after the cells incubated with NLC without OA for 4 h. When the incubation time extended to 12 h, the obvious fluorescence was observed inside A549 cells. Moreover, after incubation with fluorescent NLC with 5 wt % OA content for 1 and 2 h, there was little fluorescence inside A549 cells; however, the significant fluorescence could not be seen until 4 h. On the other hand, there was already significant fluorescence inside A549 cells after incubation with fluorescent NLC with 10 % OA content for 4 h and fluorescent NLC with 20 wt % OA content for 2 h.

From Fig. 5, it was also found that the NLC were accumulated in the cytoplasm after uptaken by A549

cells, which was consistent with the report of literature (Benis et al. 1994). As the microtubules in cytoplasm are the molecular target site of PTX, NLC are appropriate to deliver PTX into cells to enhance the target effect.

For further quantitative evaluation of the cellular uptakes of NLC, the measurement of fluorescence intensity inside cells was carried out after the cells were incubated with fluorescent NLC. Figure 6 shows fluorescence uptake percentage of NLC with different OA contents in different incubation times. The result of fluorescence quantity was consistent with the images observed from fluorescence microscopy. The cellular uptakes of NLC were time-dependent since fluorescence intensity increased with the incubation time. From Fig. 6, it was also clear that the cellular uptake percentage of NLC enhanced with the increase of OA content after 4 h. However, within 2 h, the cellular uptake percentage of NLC with 5 wt % OA content was little higher than that of NLC with 10 wt % OA content, which just explained that there was little fluorescence inside A549 cells after incubation with fluorescent NLC with 5 wt % OA content for 1 and 2 h.

Figure 7 shows the fluorescence images and fluorescence intensity after the cells were incubated with NLC (10 wt % OA content) with different concentrations for 12 h. As shown in Fig. 7, the fluorescence intensity was increased with the incubation concentration of NLC at the same incubation time. This result

Fig. 5 Fluorescence image after the cells were incubated with the fluorescent NLC (the concentrations of NLC were 100 μg mL^{-1}) with different OA contents. **a** NLC with 0 wt % OA; **b** NLC with 5 wt % OA; **c** NLC with 10 wt % OA; **d** NLC with 20 wt % OA. Original magnification ×40
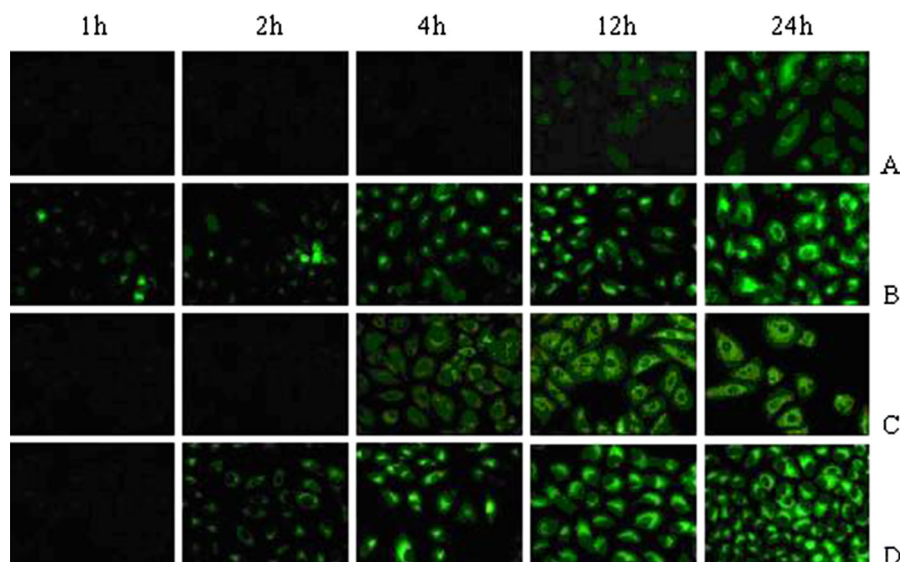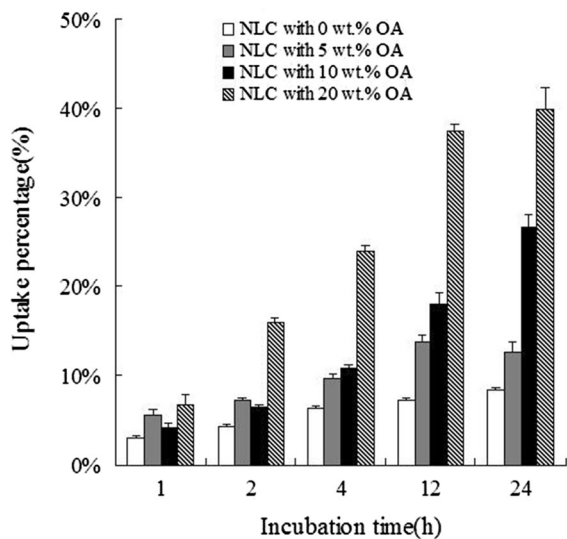
Fig. 6 The cellular uptake percentages of fluorescent NLC having different OA contents in A549 cells. The concentrations of NLC were 100 μg mL^{-1}, Mean ± SD, $n = 3$

shows that the cellular uptakes of NLC were meanwhile concentration-dependent.

Intracellular drug concentration determination

Figure 8 shows the cellular uptake percentage of PTX at different incubation times when the cells were incubated with Taxol and PTX-loaded NLC with 0–20 wt % OA. Due to great cell death after incubating cells with drug for 24 h, we limit measurement time to 24 h for reducing the experimental error. Incubating cells with Taxol within 24 h, as time prolonged, the intracellular drug concentration increased, but the drug uptake percentage only reached to 7.6 wt % (24 h) as highest value. On the other hand, with the same incubation time, the cellular uptake percentages of PTX loaded in NLC were higher than that of Taxol. The cellular uptake percentages of PTX loaded in NLC could be increased with the increase of OA content, and the drug uptake percentage could be reached to 14.3, 24.8, 30.1, and 33.8 wt % (NLC with 0, 5, 10, and 20 wt % OA content, 24 h) as highest value, respectively.

Discussion

In this study, we prepared NLC by the method of solvent dispersion, and the sizes of obtained NLC

depended on the OA content in lipid material either directly or indirectly. Directly, PTX-loaded NLC with 20 wt % OA showed a particle size decrease against PTX-loaded NLC with 10 wt % OA. As reported in previous research (Hu et al. 2005), the higher OA content led to the formation of spherical nanoparticles with smaller particle size. In this case, the particle size was mainly influenced by the OA content. Indirectly, as some researchers have reported that the particle size related with the DL, the higher DL had larger particle size (Maschke et al. 2007). Therefore, PTX-loaded NLC with 0, 5, and 10 wt % OA show a size increase because the DL increased with the increase of OA content. In addition, the sizes of PTX-loaded NLC were higher than that of fluorescent ones, which could be caused by two reasons as follows. Firstly, the incorporation of drug into NLC increased the amount of solid phase. Secondly, as the PTX is hydrophobic, and the FITC fragment of FITC–ODA is hydrophilic, the incorporation of FITC–ODA could enhance the surface hydrophilicity of NLC, and form steric hindrance to stable NLC. As a result, the sizes of fluorescent NLC were smaller than that of PTX-loaded NLC.

The EE and DL of PTX-loaded NLC were higher than PTX-loaded SLN, and further, improved with the increase of OA content. It was reported that the incorporation of liquid lipid to solid lipid could lead to massive crystal order disturbance, and the resulting matrix of lipid particles indicates great imperfections in the crystal lattice and leaves enough space to accommodate drug molecules, thus leading to improved drug EE and DL capacity (Jenning et al. 2000a). When OA content increased, the rate of imperfections in the crystal lattice also increased, thus leaving more space to accommodate drug molecules (Müller et al. 2002a).

According to the TEM images, NLC with 10 wt % OA content appeared in the formation of spherical nanoparticles. On the contrary, NLC without OA content (0 wt %) appeared in quasi-sphere and cylinder-like irregular shapes. This result was probably related with different viscosities of OA and MS. However, the particle size of NLC with 10 wt % OA content was larger than NLC without OA content, which may be owing to the increasing DL.

AFM technique has been widely applied to obtain the size (Gualbert et al. 2003), shape (Shahgaldian et al. 2003), and surface morphological (Mu and Feng 2002) information of nanoparticles. It is capable of

Fig. 7 Fluorescence image and intensity after A549 cells were incubated with the fluorescent NLC having 10 wt % OA for 12 h. **a** The concentrations of NLC were 50 μg mL^{-1}; **b** The concentrations of NLC were 100 μg mL^{-1}; **c** The concentrations of NLC were 200 μg mL^{-1} **d** The fluorescence intensity. Mean ± SD, $n = 3$
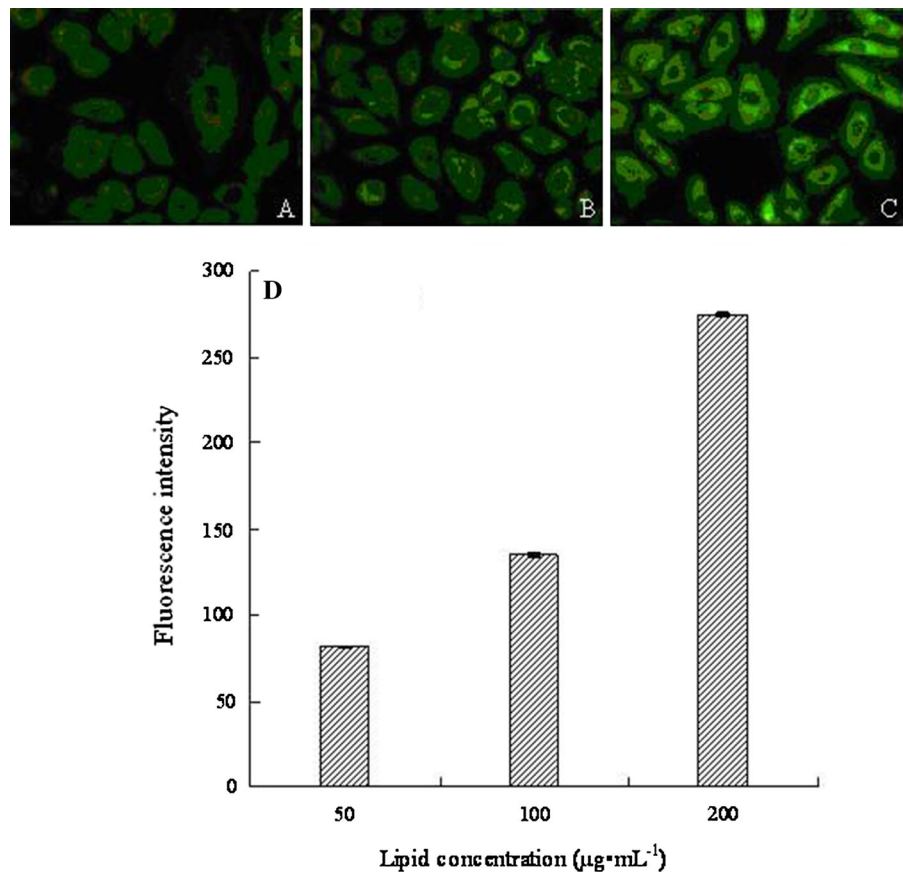

providing a contrastive and three-dimensional image of the samples and found to be a valuable tool to characterize the templates and core–shell particles (Chávez et al. 2008). The NLC system showed a low height value that indicated that they flattened but not collapsed on the substrate after solvent evaporation, suggesting a non-rigid interior. However, with OA-enriched outer layers, NLC were less severely flattened than SLN, suggesting that the shape of NLC was more spherical than that of SLN.

The release rate of PTX-loaded NLC was faster than PTX-loaded SLN, and further, accelerated with the increase of OA content. As reported in our previous study, when solvent diffusion method at 70 °C was applied to produce NLC, liquid lipid was not homogenously distributed in the matrix of nanoparticles. Instead, most of liquid lipid was located at the shell of the nanoparticles and left little or no liquid lipid entrapped into the core during the cooling process from melted lipid droplet to solid

nanoparticles (Hu et al. 2005). The OA-enriched outer layers possessed a soft and considerable higher solubility for lipophilic drug (Mühlen et al. 1996), and thus, PTX, a kind of lipophilic drug, was easily loaded with higher amount, and could easily released by the drug diffusion or the matrix erosion manners.

According to the results, we concluded that the cellular drug effect of NLC could be enhanced; however, whether and in what extent NLC could deliver PTX into target cells were still dubious. Thus, the cellular uptakes of fluorescent NLC and PTX delivered by NLC were investigated.

By investigating cellular uptakes of fluorescent NLC, the ability of NLC to be uptaken by A549 was NLC with 20 wt % OA content >NLC with 5 wt % OA content, NLC with 10 wt % OA content >NLC with 0 wt % OA content. As reported previously (Tranchant et al. 1997), the affinity of fatty acid with cell membrane related to the length and the saturation degree of its carbon chain. OA is a kind of unsaturated
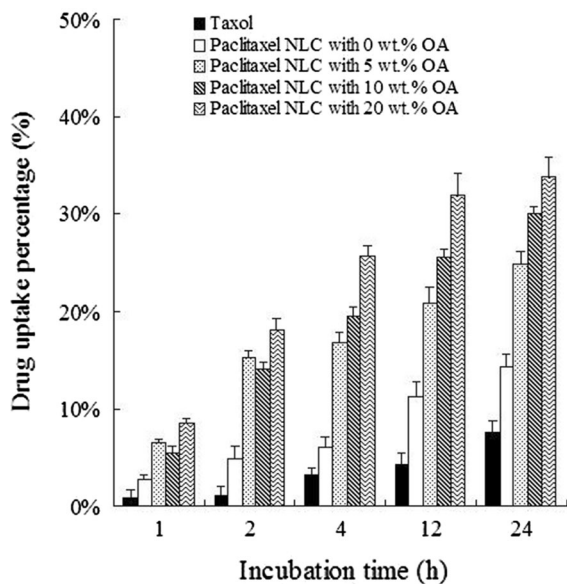
Fig. 8 The drug uptake percentage against incubation time after the cells were incubated with Taxol, PTX-loaded NLC with 0 wt % OA, PTX-loaded NLC with 5 wt % OA, PTX-loaded NLC with 10 wt % OA, and PTX-loaded NLC with 20 wt % OA. Mean ± SD, $n = 3$

fatty acid; its affinity with cell membrane is stronger than saturated fatty acid-MS, and thus, the affinity of mixture lipid is stronger than single saturated fatty acid. In addition, according to DSC analysis, the melting point of mixture lipid was lower than single saturated fatty acid (Hu et al. 2005), and the cells tend to uptake fatty acid with lower melting point. Based on the two reasons above, mixing liquid lipid OA with solid lipid can facilitate the cellular uptake of NLC. Moreover, as OA content increased, the affinity of fatty acid with cell membrane enhanced, and its melting point decreased (Hu et al. 2005), and thus, the cellular uptake of NLC enhanced accordingly.

However, in the first 2 h, the cellular uptake percentage of NLC with 5 wt % OA content was little higher than that of NLC with 10 wt % OA content. As our previous literature reported (Ding et al. 2004), after modified with PEG2000, the surface of MS SLN showed a great deal of roughness, which accelerated the endocytosis of SLN by A549 cells. Except for the factor of melting point and unsaturation degree, the ability of cellular uptake may be related with surface roughness degree of nanoparticles. According to our previous research (Hu et al. 2005), the higher OA content reduced the viscosity inside NLC and

consequently, reduced the surface tension to form smaller and smoother surface particles. Therefore, the surface roughness degree of NLC was NLC with 5 wt % OA content >NLC with 10 wt % OA content >NLC with 20 wt % OA content. Within 2 h, the factor of surface roughness degree could be in the predominance, and thus, the cellular uptake percentage of NLC with 5 wt % OA content was little higher than that of NLC with 10 wt % OA content. But after 2 h, the factor of OA content could be in the predominance, and thus, the cellular uptake percentage of NLC with 10 wt % OA content was higher than NLC with 5 wt % OA content. Therefore, the cellular uptake percentage of NLC was still proportional to the OA content.

Figure 8 shows the cellular uptake percentage of PTX at different incubation times when the cells were incubated with Taxol and PTX-loaded NLC with 0–20 wt % OA. It was clear that the cellular uptake percentages of PTX loaded in NLC were higher than that of Taxol, and further increased as the OA content increased. However, as the cellular uptake percentage of blank NLC with 5 wt % OA content was higher than that of blank NLC with 10 wt % OA content within 2 h (Fig. 6), the drug release behavior of drug-loaded NLC with 5 wt % OA was almost the same as the drug-loaded NLC with 10 wt % OA (Fig. 4), thus led to the drug uptake percentage of the former was higher than that of the latter (Fig. 8) after incubating with A549 cells for 1 and 2 h.

It was reported that the drug concentration internalized into cells could be enhanced by fast endocytosis of nanoparticles carrier and drug release in cells, and the higher drug concentration internalized into cells, leading to the better drug effect (Serpe et al. 2004). According to the results above, as a whole, the ability of NLC to be uptaken enhanced, and the PTX release rate became faster when the OA was incorporated into nanoparticles and further accelerated with the increase of the OA content, leading to PTX concentration increase. As the drug concentration increase in the target cells is the key point for cytotoxicity enhancement, the cytotoxicity of PTX was enhanced by NLC and further enhanced by increasing OA content.

Although we have gained the good results in vitro, it has to be taken into account the possibility to functionalize NLC for targeted drug delivery in vivo. Up to now, various targeting molecules have been

applied to target PTX to tumor tissues, such as folic acid (Zhang et al. 2008), RGD (Zhan et al. 2010), biotin (Heo et al. 2012), and hyaluronic acid (Yang et al. 2013). Therefore, in further studies, we will include a recognition element for targeted drug delivery in vivo to assess the specific clinical application potential of NLC.

Conclusion

The incorporation of OA into solid lipid matrix could not only improve the PTX EE and loading capacity, but also accelerate the cellular uptake and the PTX delivery. Therefore, by the encapsulation of NLC, the cytotoxicity of PTX could be enhanced, and further enhanced by increasing OA content in NLC. These results indicated that the NLC obtained in this study could potentially be exploited as an anticancer drug carrier for the targeting therapy.

References

Benis S, Chapey C, Couvreur P, Robert J (1994) Enhanced cytotoxicity of doxorubicin encapsulated in poly-isohexylcyanoacrylate nanospheres against multi-drug resistant cells in culture. Eur J Cancer 30A:89–93

Brigger I, Dubernet C, Couvreur P (2002) Nanoparticles in cancer therapy and diagnosis. Adv Drug Deliv Rev 54:631–651

Castelli F, Puglia C, Sarpietro MG, Rizza L, Bonina F (2005) Characterization of indomethacin-loaded lipid nanoparticles by differential scanning calorimetry. Int J Pharm 304:231–238

Chávez JL, Wong JL, Duran RS (2008) Core-Shell Nanoparticles: characterization and study of their use for the encapsulation of hydrophobic fluorescent dyes. Langmuir 24:2064–2071

Ding JC, Hu FQ, Yuan H (2004) Uptake of monostearin solid lipid nanoparticles by A549 cells. Acta Pharm Sin 39:876–880

Drummond DC, Meyer O, Hong K, Kirpotin DB, Papahadjo-poulos D (1999) Optimizing liposomes for delivery of chemotherapeutic agents to solid tumors. Pharmacol Rev 51:691–744

Garrec DL, Ranger M, Leroux JC (2004) Micelles in anticancer drug delivery. Am J Drug Deliv 2:15–42

Gelderblom H, Verweij J, Nooter K, Sparreboom A (2001) Sparreboom. Cremophor EL: the drawbacks and advantages of vehicle selection for drug formulation. Eur J Cancer 37:1590–1598

Gualbert J, Shahgaldian P, Coleman AW (2003) Interactions of amphiphilic calix[4] arene-based solid lipid nanoparticles with bovine serum albumin. Adv Drug Deliv Rev 57:69–73

Heo DN, Yang DH, Moon HJ, Lee JB, Bae MS, Lee SC, Lee WJ, Sun IC, Kwon IK (2012) Gold nanoparticles surface-functionalized with paclitaxel drug and biotin receptor as theranostic agents for cancer therapy. Biomaterials 33:856–866

Hu FQ, Jiang SP, Du YZ, Yuan H, Ye YQ, Zeng S (2005) Preparation and characterization of stearic acid nano-structured lipid carriers by solvent diffusion method in an aqueous system. Colloids Surf B 45:167–173

Hu FQ, Ren GF, Yuan H, Du YZ, Zeng S (2006) Shell cross-linked stearic acid grafted chitosan oligosaccharide self-aggregated micelles for controlled release of paclitaxel. Colloids Surf B 50:97–103

Hu Y, Zheng XT, Chen JS, Zhou MJ, Li CM, Lou XW (2011) Silica-based complex nanorattles as multifunctional carrier for anticancer drug. J Mater Chem 21:8052–8056

Jenning V, Gohla SH (2001) Encapsulation of retinoids in solid lipid nanoparticles (SLN). J Microencapsul 18:149–158

Jenning V, Andreas FT, Gohla SH (2000a) Characterisation of a novel solid lipid nanoparticle carrier system based on binary mixtures of liquid and solid lipids. Int J Pharm 199:167–177

Jenning V, Mader K, Gohla SH (2000b) Solid lipid nanoparticles (SLNTM) based on binary mixtures of liquid and solid lipids: a 1HNMR study. Int J Pharm 20:15–21

Jores K, Mehnert W, Drechsler M, Bunjes H, Johann C, Mäder K (2004) Investigations on the structure of solid lipid nanoparticles (SLN) and oil-loaded solid lipid nanoparticles by photon correlation spectroscopy, field-flow fractionation and transmission electron microscopy. J Control Release 95:217–227

Maschke A, Becker C, Eyrich D, Kiermaier J, Blunka T, Göpferich A (2007) Development of a spray congealing process for the preparation of insulin-loaded lipid micro-particles and characterization. Eur J Pharm Biopharm 65:175–187

Miao J, Du YZ, Yuan H, Zhang XG, Hu FQ (2013) Drug resistance reversal activity of anticancer drug loaded solid lipid nanoparticles in multi-drug resistant cancer cells. Colloids Surf B 110:74–80

Montasser I, Fessi H, Coleman AW (2002) AFM imaging of novel type of polymeric colloidal nanostructures. Eur J Pharm Biopharm 54:281–284

Mu L, Feng SS (2002) Vitamin E TPGS used as emulsifier in the solvent evaporation/extraction technique for fabrication of polymeric nanospheresfor controlled release of paclitaxel (Taxol). J Control Release 80:129–144

Mühlen AZ, Mühlen EZ, Niehus H, Mehnert W (1996) Atomic force microscopy studies of solid lipid nanoparticles. Pharma Res 13:1411–1416

Müller RH, Jacobs C, Kayser O (2001) Nanosuspensions as particulate drug formulations in therapy Rationale for development and what we can expect for the future. Adv Drug Deliv Rev 47:3–19

Müller RH, Radtke M, Wissing SA (2002a) Nanostructured lipid matrices for improved microencapsulation of drugs. Int J Pharm 242:121–128

Müller RH, Radtke M, Wissing SA (2002b) Solid lipid nanoparticles (SLN) and nanostructured lipid carriers (NLC) in cosmetic and dermatological preparations. Adv Drug Deliv Rev 54:S131–S155

Serpe L, Catalano MG, Cavalli R, Ugazio E, Bosco O, Canaparo R, Muntoni E, Frairia R, Gasco MR, Eandi M, Zara GP (2004) Cytotoxicity of anticancer drugs incorporated in solid lipid nanoparticles on HT-29 colorectal cancer cell line. Eur J Pharm Biopharm 58:673–680

Shahgaldian P, Silva ED, Anthony W (2003) Para-acyl-calix-arene based solid lipid nanoparticles (SLNs): a detailed study of preparation and stability parameters. Int J Pharm 253:23–28

Souto EB, Wissing SA, Barbosa CM (2004a) Development of a controlled release formulation based on SLN and NLC for topical clotrimazole delivery. Int J Pharm 278:71–77

Souto EB, Wissing SA, Barbosa CM, Müller RH (2004b) Evaluation of the physical stability of SLN and NLC before and after incorporation into hydrogel formulations. Eur J Pharm Biopharm 58:83–90

Tranchant T, Besson P, Hoinard C, Delarue J, Antoine JM, Couet C, Goré J (1997) Mechanisms and kinetics of α-linolenic acid uptake in Caco-2 clone TC7. Biochim Biophys Acta 1345:151–161

Yang XY, Li YX, Li M, Zhang L, Feng LX, Zhang N (2013) Hyaluronic acid-coated nanostructured lipid carriers for targeting paclitaxel to cancer. Cancer Lett 334:338–345

Yuan H, Miao J, Du YZ, You J, Hu FQ, Zeng S (2008) Cellular uptake of solid lipid nanoparticles and cytotoxicity of encapsulated paclitaxel in A549 cancer cells. Int J Pharm 348:137–145

Zhan CY, Gu B, Xie C, Li J, Liu Y, Lu WY (2010) Cyclic RGD conjugated poly(ethylene glycol)-co-poly(lactic acid) micelle enhances paclitaxel antiglioblastoma effect. J Control Release 143:136–142

Zhang XG, Miao J, Dai YQ, Du YZ, Yuan H, Hu FQ (2008) Reversal activity of nanostructured lipid carriers loading cytotoxic drug in multi-drug resistant cancer cells. Int J Pharm 361:239–244